NANO LETTERS

2007
Vol. 7, No. 7
2101−2107

Metal-Enhanced Single-Molecule Fluorescence on Silver Particle Monomer and Dimer: Coupling Effect between Metal Particles

Jian Zhang, Yi Fu, Mustafa H. Chowdhury, and Joseph R. Lakowicz*

Center for Fluorescence Spectroscopy, University of Maryland School of Medicine, Department of Biochemistry and Molecular Biology, 725 West Lombard Street, Baltimore, Maryland 21201

Received May 9, 2007; Revised Manuscript Received June 4, 2007

ABSTRACT

We prepared silver particle dimers with single Cy5 molecules localized between coupled metal particles. The silver particles with a 20 nm diameter were chemically bound with single-stranded oligonucleotides. The dimers were formed by hybridization with double-length single-stranded oligonucleotides that contained single Cy5 molecules. The image analysis revealed that the single-molecule fluorescence was enhanced 7-fold on the metal monomer and 13-fold on the metal dimer relative to the free Cy5-labeled oligonucleotide in the absence of metal. The lifetimes were shortened on the silver monomers and further shortened on the silver dimers, demonstrating the near-field interaction mechanism of fluorophore with the metal substrate. Finite-difference time-domain (FDTD) calculations were employed to study the distribution of electric field near the metal monomer and dimer. The coupling effect of metal particle on the fluorescence enhancement was discussed.

A fluorophore behaves as an oscillating dipole to radiate energy as fluorescence.[1,2] When the fluorophore is localized near a metal surface, fluorescence can be enhanced, which we define as metal-enhanced fluorescence (MEF).[3−9] MEF is known to occur primarily due to the near-field interactions of the excited-state fluorophore with the local electric fields on the metal particle that is induced by incident light.[8,9] This approach is attracting interest in developing novel nanoscale structures for biological and clinical fluorescence sensing.[10,11]

Single-molecule detection (SMD) is regarded as a valuable method to study fluorophore−metal interaction at the single-molecule level because of its ability to bypass ensemble averaging and allow resolution of actual distributions of the spectral parameters.[12] Such details of the underlying distribution become crucially important when the system is heterogeneous.[13] The brightness or emission rate determines the observability of a single molecule and the photostability determines the time that it can be observed prior to photobleaching. Hence it is crucial to extend the improved ensemble spectral properties to single-molecule level. Herein, we utilized the SMD technology to investigate MEF on the metal particle at single-fluorophore level.[14] Experimentally, the silver particles were synthesized by a wet method.[15] The single-stranded oligonucleotides were first chemically bound to the metal particles, and the fluorophore-labeled complementary oligonucleotides (oligonucleotides 2 in Scheme 1) were bound to the metal particles by hybridization with the bound oligonucleotides on the metal particles.[16] According to Schatz et al., the electric field in the space between the coupled metal particles is more intense than that of a monomer.[17] Thus, we are interested in the coupling effect of the metal dimers on MEF. In this system, the metal dimers were synthesized and labeled by hybridization of the double-length labeled oligonucleotides (oligonucleotides 3 in Scheme 1) with the bound oligonucleotides on the metal particles.

We correlated the experimental results with numerical calculations. The finite-difference time-domain (FDTD) technique is an implementation of Maxwells's time-dependent curl equations for solving the temporal variation of electromagnetic waves within a finite space that contains a target of arbitrary shape and has recently become the start-of-the-art method for solving Maxwell's equations for complex geometries.[18−21] Because FDTD is a direct time and space solution, it offers the user a unique insight into all types of problems in electromagnetics and photonics. It can also be used to obtain the frequency solution by exploiting Fourier transforms, thus a full range of useful quantities in addition to fields around particles can be calculated, such as the complex Poynting vector and the transmission/reflection of light. In the FDTD technique, Maxwell's curl equations are discretized by using finite-difference approximations in

* Corresponding author. E-mail: lakowicz@cfs.umbi.umd.edu.

10.1021/nl071084d CCC: $37.00
Published on Web 06/20/2007

Scheme 1. The Tiopronin-coated Silver Particle Was Succinimidylated via Ligand Exchange, Covalently Bound with Aminated Single-Stranded Oligonucleotide by Condensation, and Fluorescently Labeled by Complementary Single-Stranded Cy5-labeled Oligonucleotide to Generate the Labeled Metal Monomer[a]

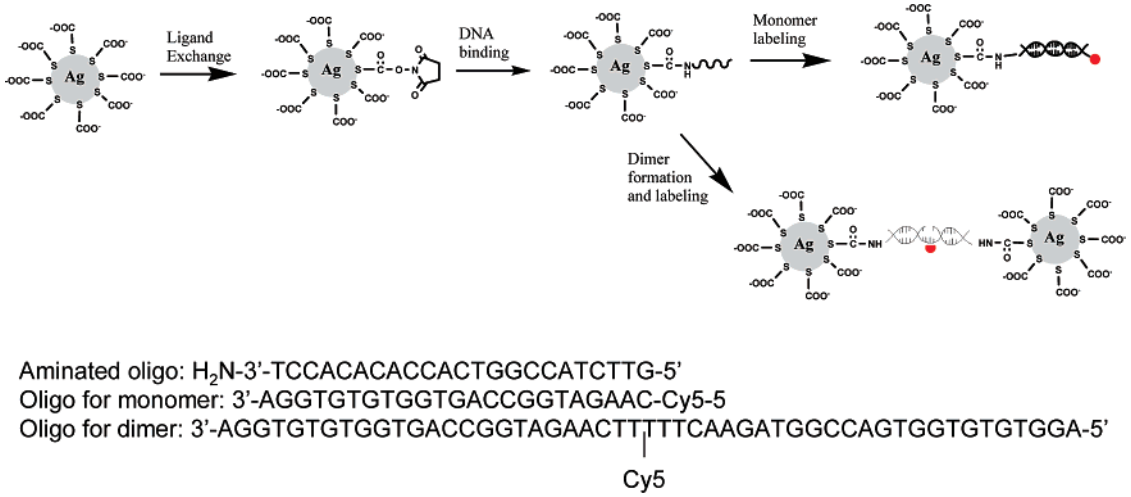

[a] The metal dimer was prepared by hybridization of double-length oligonucleotide with the bound oligonucleotide on the metal particle. Oligonucleotide sequences that were used in the experiments are given.

both time and space that are easy to program and are accurate.[18−21] To achieve high accuracy for realizing the spatial derivatives involved, the algorithm positions the components of the electric and magnetic field about a unit cell of the lattice that constitutes the FDTD computational domain. Each individual cube in the grid is called the Yee cell as it was first designed elegantly by Yee.[18] Herein, we estimated the distribution of electric field near the metal monomer and dimer to explain single-molecule MEF of on these metal particles.

Experimental Section. All reagents and spectroscopic grade solvents were used as received from Fisher or Aldrich. RC dialysis membrane (MWCO 50 000) was obtained from Spectrum Laboratories, Inc. Nanopure water (>18.0 M Ω.cm), purified using Millipore Milli-Q gradient system, was used in all experiments. (2-Mercapto-propionylamino) acetic acid 2,5-dioxo-pyrrolidin-1-ylester was synthesized as previous reported.[22] Oligonucleotides were synthesized by the Biopolymer Laboratory in the University of Maryland at Baltimore.

Preparing Tiopronin-Coated Metal Nanoparticles and Binding Aminated Single-Stranded Oligonucleotides. Tiopronin-coated silver nanoparticles were prepared using a modified Brust reaction with a mole ratio of tiopronin/silver nitrate = 1/6 in methanol using reduction by an excess amount of sodium borohydride.[23] After filtration, the residual precipitated particles were washed thoroughly with methanol and acetone. Particle (1 mg/mL) and tiopronin (10 mM) were then co-dissolved in water at pH = 7.0, and the solution was stirred for 24 h for particle annealing.[24] The water was removed under vacuum, and the residual was washed thoroughly with methanol and acetone. The residual solids were further purified by dialysis against water.

The tiopronin-coated silver particles were succinimidylated by a ligand exchange reaction.[24,25] (2-Mercapto-propionylamino) acetic acid 2,5-dioxo-pyrrolidin-1-ylester (2×10^{-8} M) and the silver particle (1 mg/mL, 4×10^{-8} M) were co-dissolved in a mixing solvent of water/methanol (v/v = 1/1) and stirred for 24 h.[16,26] The suspension was removed by centrifugation at 8000 rpm. The residue was washed by methanol and water respectively and then dispersed in water at pH = 7.0.

Binding DNA on the Metal Particles and Preparing the Labeled Metal Monomers and Dimers by Hybridization with DNA. The animated oligonucleotides (oligonucleotide 1 in Scheme 1) were chemically bound onto the silver particles by co-dissolving the oligonucleotides (1 μM) and succinimidylated particles (1 mg/mL, 4×10^{-8} M) in water with continuous stirring for 24 h.[16] The suspension was removed by centrifugation at 8000 rpm. The residue was washed with water and then dispersed in 50 mM PBS buffer solution at pH = 7.2. The oligonucleotide-bound particles were further purified by dialysis against buffer solution to remove all free impurities (MWCO 50 000). The labeled metal monomers were achieved by the hybridizations between the bound oligonucleotide 1 and labeled oligonucleotide 2 at a molar ratio of particle/target oligonucleotide = 1/1, and the metal dimers were achieved by hybridization between the bound oligonucleotide 1 and labeled double-length oligonucleotide 3 in buffer solution at a molar ratio of particle/oligonucleotide = 2/1. The hybridizations were performed for 24 h. Then the suspension was removed by centrifugation at 8000 rpm, and the residue was washed with buffer solution.

Spectra, Lifetime, and TEM Measurements. Absorption spectra were monitored with a Hewlett-Packard 8453 spectrophotometer. Ensemble fluorescence spectra were recorded in solution with a Cary Eclipse fluorescence spectrophotometer. All single-molecule studies were performed using a time-resolved confocal microscope (MicroTime 200, PicoQuant). Immobilization of nanoparticles on glass coverslips was achieved by adding 20 μL of 100× diluted Cy5−nanoparticle suspension onto an aminosilanized coverslip

following by spin drying at 4000 rpm. A single-mode pulsed laser diode (635 nm, 100 ps, 40 MHz) (PDL800, PicoQuant) was used as the excitation light. The collimated laser beam was spectrally filtered by an excitation filter (D637/10, Chroma) before directing into an inverted microscope (Olympus, IX 71). An oil immersion objective (Olympus, 100×, 1.3 NA) was used both for focusing laser light onto the sample and collecting fluorescence emission from the sample. The fluorescence that passed a dichroic mirror (Q655LP, Chroma) was focused onto a 75 μm pinhole for spatial filtering to reject out-of-focus signals and then reached the single-photon avalanche diode (SPAD) (SPCM-AQR-14, Perkin-Elmer Inc). Images were recorded by raster scanning (in a bidirectional fashion) the sample over the focused spot of the incident laser with a pixel integration of 0.6 ms. The excitation power into the microscope was maintained at less than 1 μW. Time-dependent fluorescence data were collected with a dwell time of 50 ms. The data was stored in a time-tagged-time-resolved (TTTR) mode, which allows recording every detected photon with its individual timing information. Instrument response function (IRF) widths of about 300 ps fwhm can be obtained in combination with a pulsed diode laser, which permits the recording of subnanosecond fluorescence lifetimes extendable to less than 100 ps with reconvolution. Lifetimes were estimated by fitting to a χ^2 value of less than 1.2 and with a residuals trace that was fully symmetrical about the zero axis. All measurements were performed in a dark compartment at room temperature.

Transmission electron micrographs (TEM) were taken with a side-entry Philips electron microscope at 120 keV. Samples were cast from water solutions onto standard carbon-coated (200−300 Å) Formvar films on copper grids (200 mesh) by placing a droplet of a 1 mg/mL aqueous sample solution on grids. The size distribution of metal core was analyzed with Scion Image Beta Release 2, counting at least 200 particles.

FDTD Calculations. Our FDTD calculations were performed using the program FDTD Solutions (version 5.0) purchased from Lumerical Solutions, Inc., (Vancouver, Canada). The calculations were performed with the parallel FDTD option on a Dell Precision PWS690 workstation with the following components: Dual Quad-Core Intel Xeon E5320 processors at 1.86 GHz and 8 GB RAM. All post-processing of FDTD data were performed using MATLAB (version 7.0) provided by Mathworks (Natick, MA). To maintain the accuracy and stability of the FDTD calculations, the smallest grid size to accurately model the prescribed system without being computationally prohibitive was obtained in an iterative fashion (convergence testing). In our implementation of FDTD, convergence testing was done by starting the first calculation with a grid size of $\lambda_0/20$, where λ_0 is the smallest wavelength expected in the simulation, and then reducing the grid size by half in sequential simulations and comparing the results of the calculations. The reduction of the grid size was stopped when we approached a grid size (Δ) where results closely match with the set of results that are obtained from half that particular grid size ($\Delta/2$).[19] The numerical implementation of Maxwell's equations in the FDTD algorithm requires that the time increment Δt have a specific bound relative to the spatial discretization Δ (as mentioned above) to ensure the stability of the time-stepping algorithm. In our implementation of FDTD, the time step of the simulation was determined by the values of the spatial grid to ensure numerical stability and the user has the flexibility to set the total time of the simulation in femtoseconds (fs).[21] Our typical simulations were ranged around 300 fs. This led to all of our simulations having an excess of 50 000 time steps. Our FDTD software had frequency domain monitors that performed discrete Fourier transforms of the time domain fields while the simulation was running. In this manner, continuous wave (CW) information was obtained at any pre-specified wavelengths for the various field components (E_x, E_y, E_z, H_x, H_y, and H_z). Additionally, the time domain monitors can provide time domain information for the various field components within the FDTD simulation region over the entire course of the simulation. At the end of the simulation, the various field components were checked to see if they decayed to zero, thus indicating that the simulation has run for a sufficiently long time for the CW information obtained by Fourier transformations to be valid.[21]

Results and Discussion. The silver particles were synthesized with the terminated carboxylic ligands and displayed good solubility and chemical stability in water. TEM images showed the silver particles were approximately homogeneous in size distribution (inset of Figure 1a). The *average* diameter of metal cores was detected to be 20 nm, and the chemical composition was estimated to be ca. $(Ag)2.5\times10^5(Tio)5.0\times10^3$.

The ligand exchange is known to occur at a mole ratio of 1:1, so (2-mercapto-propionylamino) acetic acid 2,5-dioxo-pyrrolidin-1-ylester was co-dissolved with the silver particle at a mole ratio of 1/2 in water to ensure loading only one succinimidylated ligand per metal particle.[16] At this molar ratio, even though the succinimidyl ligands were completely transferred onto the metal particles, at the most, there were only half of the metal particles that were single-succinimidylated. This strict limitation of a single succinimidyl ligand on the metal particle may guarantee that it is definitely bound by a single aminated oligonucleotide in the following surface reaction and then labeled by the single fluorophore through hybridization with the long-chain oligonucleotide. We did not separate the succinimidylated particles from the unmodified particles after the surface reactions because only the succinimidylated particle could be bound by the aminated DNA and then dimerized via the hybridization with the long-chain labeled DNA. Because both the unmodified particles and DNA are negatively charged on their surfaces, nonspecific interactions between them were supposed to occur and result in the aggregation of metal particles.

Absorbance spectra of silver particles were performed in 10 mM PBS buffer solution. It was shown that the tiopronin-coated silver particles displayed a metal plasmon absorbance at 401 nm (Figure 1). The surface reactions including the ligand exchange and oligonucleotide binding did not significantly alter the absorbance spectrum of the metal particles,

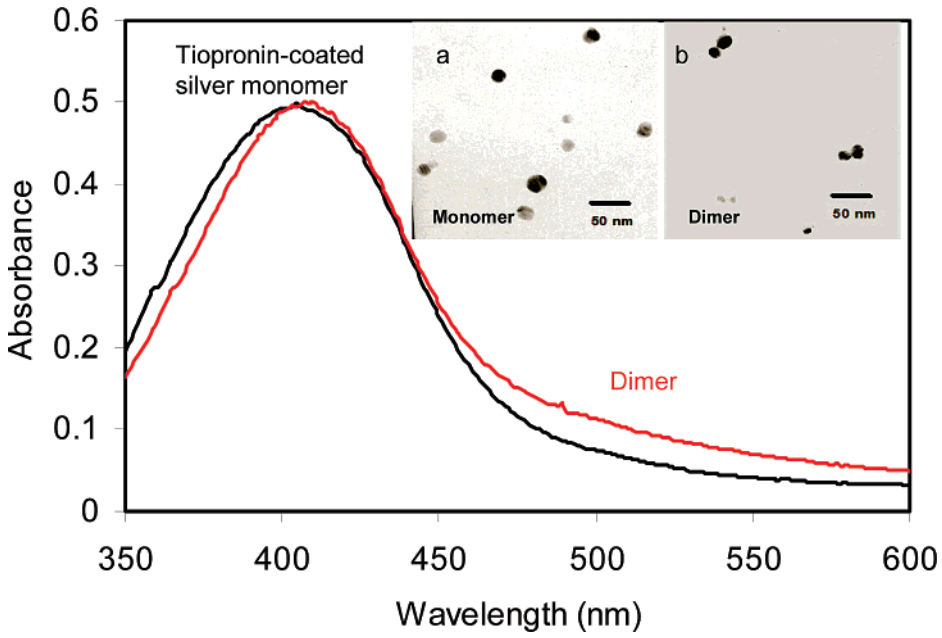

Figure 1. Absorbance spectra of tiopronin-coated silver particles and the metal dimers that were formed by hybridization of double-length oligonucleotide with the bound oligonucleotide on the metal particle with the different metal core sizes. Transmission electron micrographs (TEM) images of metal monomers and dimers are given in the insets (a) and (b), respectively.

indicating that only a few ligands were involved. Simultaneously, the TEM images of metal particles showed no significant changes after these reactions occurred. As described above, the metal monomers and dimers were synthesized by hybridization of oligonucleotides 2 and 3, respectively, with the bound oligonucleotide 1 on the metal particles in 50 mM PBS buffer solution at pH = 7.2 (Scheme 1).[16,22] The hybridization on the metal monomers did not alter the absorbance wavelength, but the hybridization on the metal dimers could result in a slight red-shifting of the metal plasmon absorbance to 403 nm (Figure 1).[27] This wavelength shift was smaller than the reported value, reflecting that only a portion of metal particles was dimerized by the hybridization. The formation of metal dimer was also verified clearly by the TEM images (inset b of Figure 1). The inset b of Figure 1 showed up the typical TEM images of formed dimers. Actually, many individual and few aggregated metal particles were also observed. When the TEM images were analyzed by at least 200 counting, it was shown that about 75% of particles exist as the monomers, 23% as the dimers, and less than 2% as the aggregates that contain more than two individuals. Because some dimer or aggregates were regarded to form occasionally when drying the solution on the grid, we thought that there were 30−40% of metal particles existing as the dimers formed by DNA hybridization. This ratio approximately consisted with the value obtained by the emission intensity

Ensemble emission spectra were first used to monitor the binding of fluorophores on the metal particles. Unbound Cy5-labeled oligonucleotide in 10 mM PBS buffer solution displayed an emission maximum at 661 nm upon excitation at 620 nm when measured in ensemble spectroscopy. The emission wavelength was slightly red-shifted to 663 nm when binding the fluorophore on either monomer or dimer metal particles, consistent with previous observations.[28] We employed metal monomers to estimate the loading number of fluorophores per metal nanoparticle. Experimentally, a known concentration metal particle in buffer solution was added to a couple drops of 0.1 N NaCN aqueous solution.[27] The metal cores were dissolved and the fluorophore-labeled oligonucleotides were released. The released fluorophores displayed an identical emission spectrum to the free oligonucleotide in the absence of metal, so the concentration of fluorophore was estimated by the emission intensity. The loading number was calculated to be ca. 0.3, indicating 30% of silver particles having one fluorophore as we required in this case.

We investigated the single-molecule spectral properties using the SMD technique on the labeled metal particles. The fluorescence was first examined for the fluorophores without the metal particles and on the metal monomers. Typical fluorescence images of a 5 μm × 5 μm region were recorded (Figure 2).[17] The recorded images provided initial and quantitative information on the brightness of single molecules. All image spots were circle-shaped, but the labeled metal monomers (Figure 2b) were much brighter than the free fluorophores in the absence of metal (Figure 2a). Histograms of the intensity were constructed by counting more than 50 molecules. Only spots displaying single-step photobleaching were included in the analysis. The time profiles of traces were collected under the excitation (Figure 3). Most traces showed clear one-step photobleaching, corresponding to the typical behavior from single fluorophores. The intensity was observed to be fairly constant until dropping abruptly to the background level in a single step. The fluorescence of single fluorophore on the metal monomers was enhanced 7-fold over the intensity of free Cy5-labeled oligonucleotide in the absence of metal. Because the scattering intensity from the unlabeled metal particles was less than 5% of the emission intensity from the free

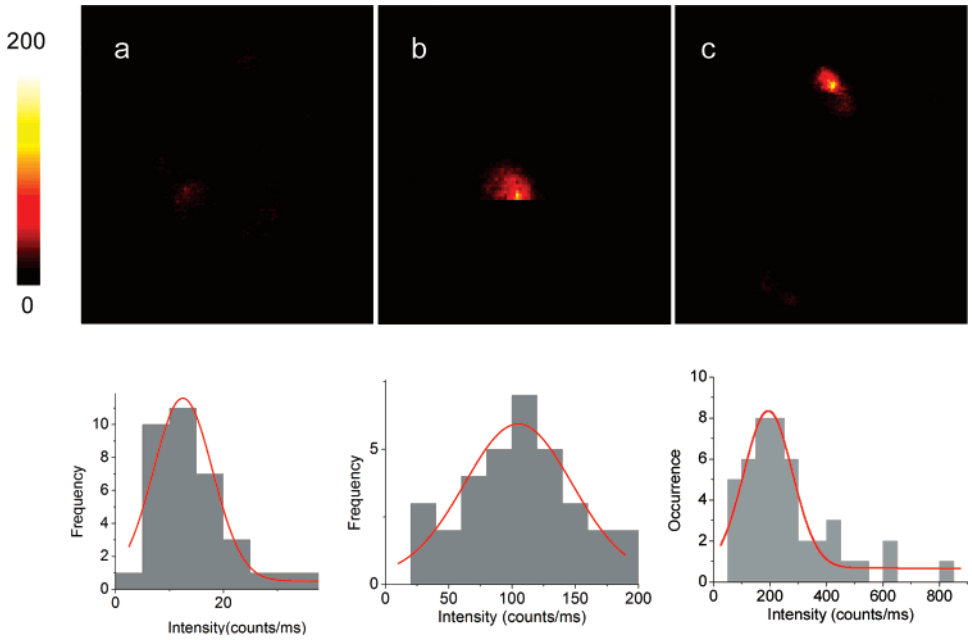

Figure 2. Respective fluorescence images of single-labeled (a) free Cy5, (b) single fluorophore on metal monomer, and (c) on metal dimer. The 5 μm $\times$ 5 μm images are 100 pixels $\times$ 100 pixels with in integration time of 0.6 ms per pixel. The corresponding histograms of emission intensity are presented.

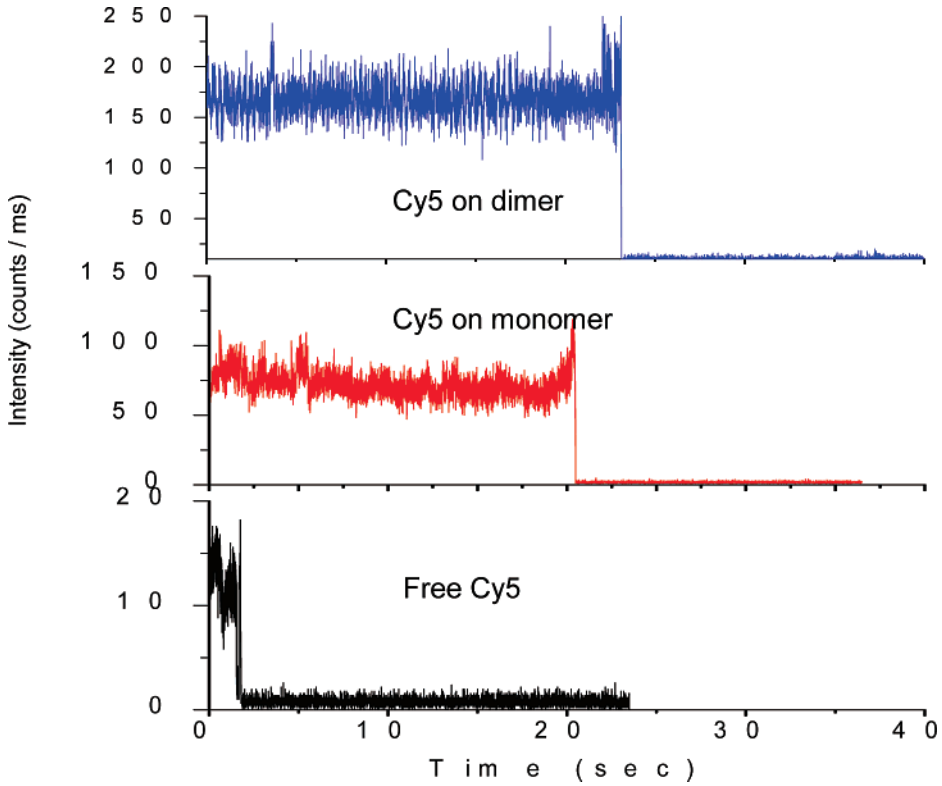

Figure 3. Respective time-traces of single Cy5-labeled oligonucleotide in the absence of metal, on metal monomer, and on metal dimer.

fluorophores, we attributed the emission enhancement to the metal-enhanced fluorescence on the metal monomers.

Next, we studied the fluorescence signal changes on the metal dimers. It was observed that, like the case of the metal monomers, the collected images on the metal dimers were also circle-shaped but became brighter (Figure 2c). The histogram of these labeled metal dimers, collected by an analogous method as the labeled metal monomers, showed a 13-fold intensity increase relative to the free fluorophores. This value was about double than the labeled metal monomers. To the best of our knowledge, this is the first experimental demonstration of the coupling effect between the metal particles that can lead to a more efficient MEF. The time trace profile of the labeled metal dimers showed a higher intensity scale than the metal monomers, and the emission persisted much longer than the free fluorophores

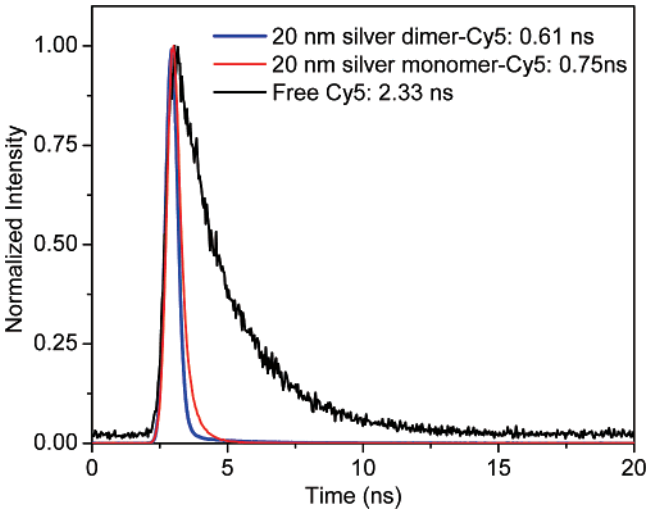

Figure 4. Emission decay curves fits for single Cy5-labeled oligonucleotide in the absence of metal, on metal monomer, and on metal dimer.

in the absence of metal. This was also observed on immobilized silver particles as islands.[14]

MEF is known to occur via an increase of the intrinsic decay rate for a fluorophore near a metal surface.[9a] As a result, the lifetime of the fluorophore should be shortened dramatically. This result is important evidence to confirm the metal−fluorophore near-field interaction. In this case, the lifetimes were derived from the time traces using time-corrected single-photon counting (TCSPC) technique and analyzed in terms of a single-exponential decay (Figure 4). The lifetime of Cy5-labeled fluorophore was estimated to be 2.3 ns in the absence of metal, shortened to be 0.75 ns on the metal monomer, and furthermore altered to 0.61 ns on the metal dimer. The difference of lifetime value was small between the labeled monomer and dimer, which may be due to the limitations in the time resolution of our instrument. But we still can conclude that the trend observed in the shortening of lifetime was consistent with the intensity enhancement on the metal particles.

The lifetime of fluorophores near metal particles can influence their photostability.[9b] A shorter lifetime results in a smaller time for photochemistry while in the excited state and thus more excitation−emission cycles prior to photobleaching. In this study, the time traces showed that both labeled metal monomers and dimers had emissions lasting for at least 20 s before bleaching, but the free fluorophore in the absence of metal had emissions lasting for only 2 s (Figure 3), indicating that the photostability of fluorophore was extended 10-fold on the metal particles.

We know that MEF occurs via a near-field interaction of the fluorophore with the metal nanoparticle. The electric field near the metal particle is an important factor that influences MEF. These fields generated near a silver particle when under illumination from incident light can be calculated by the FDTD technique (Figure 5).[18−21] In this case, the hybridized DNA duplexes are regarded as rigid rods that separate the fluorophores and the surfaces of metal cores. The oligonucleotides on the metal monomer contain 23 base pairs that are about 8 nm long. So the MEF efficiency of the labeled metal monomers can be assumed to depend on the intensity distribution profile of the electric field at distance of 8 nm from the metal core. Our FDTD calculations reveal that the electric field intensity on the metal monomer decays significantly at this distance, so the MEF efficiency cannot be expected to be significant. However, our calculations also show that the electric field intensity in the space between the metal dimers is increased due to the coupling effect of metal particles, which can result in higher MEF efficiencies on the metal dimers. Although it is difficult to directly compare the experimental results of the metal

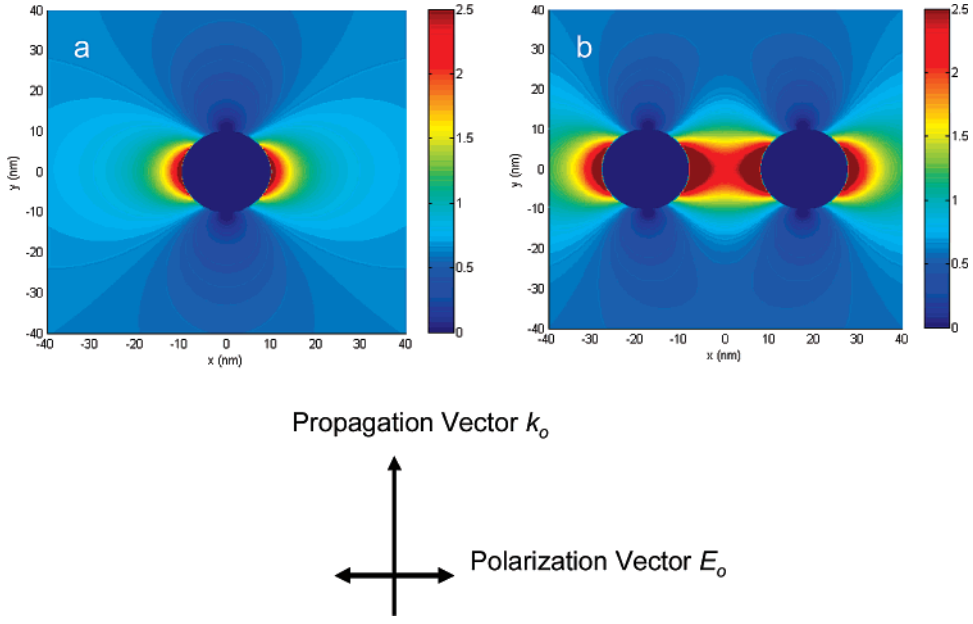

Figure 5. Electric fields near silver (a) monomer and (b) dimer were calculated by FDTD model under an incident light of 635 nm. Note the incident light is propagating along the *y*-axis and is polarized along the *x*-axis.

monomer and dimer to the FDTD calculations in a quantitative manner, we still see qualitative agreements between our experimental observations and FDTD calculations. Of course, a complete numerical analysis would require further considerations of the field induced by the fluorophore.

In this paper, we studied MEF at the single-fluorophore level on silver monomers and dimers. The silver particles were fluorescently labeled by Cy5 via DNA hybridization. Single-molecule fluorescence images were recorded using scanning confocal microscopy. The emission image analysis of single fluorophores showed a 7-fold enhancement on the metal monomers and a 13-fold enhancement on the metal dimers when compared to the free fluorophore in the absence of metal. The lifetime results verified the near-field interaction mechanism of fluorophore with the metal particle. The electric fields near the metal monomer and dimer were calculated by the FDTD method and were further employed to explain the coupling effect between the metal particles. In subsequent studies, we will investigate the effect of different core sizes of silver particles and different distances between the coupled particles.

Acknowledgment. This research was supported by a grant from NIH, HG-02655, NCRR, and RR-08119.

References

(1) Lakowicz, J. R. *Principles of Fluorescence Spectroscopy*, 3rd ed.; Springer: New York, 2006.
(2) Lakowicz, J. R.; *Emerging Biomedical Application of Time-Resolved Fluorescence Spectroscopy*; Topics in Fluorescence Spectroscopy, Vol. 4, Probe Design and Chemical Sensing; Lakowicz, J. R., Ed.; Plenum Press: New York, 1994.
(3) Gryczynski, I.; Malicka, J.; Shen, Y. B.; Gryczynski, Z.; Lakowicz, J. R. *J. Phys. Chem. B* **2002**, *106*, 2191. (b) Aslan, K.; Huang, J.; Wilson, G. M.; Geddes, C. D. *J. Am. Chem. Soc.* **2006**, *128*, 4206.
(4) (a) Sokolov, K.; Chumanov, G.; Cotton, T. M. *Anal. Chem.* **1998**, *70*, 3898. (b) Shen, Y.; Swiatkiewicz, J.; Lin, T.-C.; Markowicz, P.; Prasad, P. N. *J. Phys. Chem. B* **2002**, *106*, 4040.
(5) (a) Lee, I.-Y. S.; Suzuki, H.; Ito, K.; Yasuda, Y. *J. Phys. Chem. B* **2004**, *108*, 19368. (b) Yonzon, C. R.; Jeoung, E.; Zou, S.; Schatz, G. C.; Mrksich, M.; Van, Duyne, R. P. *J. Am. Chem. Soc.* **2004**, *126*, 12669.
(6) (a) Song, J.-H.; Atay, T.; Shi, S.; Urabe, H.; Nurmikko, A. V. *Nano Lett.* **2005**, *5*, 1557. (b) Kawasaki, M.; Mine, S. *J. Phys. Chem. B* **2005**, *109*, 17254.
(7) (a) Kummerlen, J.; Leitner, A.; Brunner, H.; Aussenegg, F. R.; Wokaun, A. *Mol. Phys.* **1993**, *80*, 1031. (b) Antunes, P. A.; Constantino, C. J. L.; Aroca, R. F.; Duff, J. *Langmuir* **2001**, *17*, 2958. (c) Kamat, P. V. *J. Phys. Chem. B* **2002**, *106*, 7729.
(8) (a) Kumbhar, A. S.; Kinnan, M. K.; Chumanov, G. *J. Am. Chem. Soc.* **2005**, *127*, 12444. (b) Hubert, C.; Rumyantseva, A.; Lerondel, G.; Grand, J.; Kostcheev, S.; Billot, L.; Vial, A.; Bachelot, R.; Royer, P.; Chang, S.-h.; Gray, S. K.; Wiederrecht, G. P.; Schatz, G. C. *Nano Lett.* **2005**, *5*, 615. (c) Millstone, J. E.; Park, S.; Shuford, K. L.; Qin, L.; Schatz, G. C.; Mirkin, C. A. *J. Am. Chem. Soc.* **2005**, *127*, 5312.
(9) (a) Lakowicz., J. R. *Anal. Biochem.* **2001**, *298*, 1. (b) Lakowicz., J. R. *Anal. Biochem.* **2005**, *337*, 171.
(10) (a) Yu, F.; Persson, B.; Lofas, S.; Knoll, W. *J. Am. Chem. Soc.* **2004**, *126*, 8902. (b) Ekgasit, S.; Thammacharoen, C.; Yu, F.; Knoll, W. *Anal. Chem.* **2004**, *76*, 2210. (c) Baluschev, S.; Yu, F.; Miteva, T.; Ahl, S.; Yasuda, A.; Nelles, G.; Knoll, W.; Wegner, G. *Nano Lett.* **2005**, *5*, 2482.
(11) (a) Futamata, M.; Maruyama, Y.; Ishikawa, M. *J. Phys. Chem. B* **2003**, *107*, 7607. (b) Sherry, L. J.; Chang, S.-H.; Schatz, G. C.; Van, Duyne, R. P.; Wiley, B. J.; Xia, Y. *Nano Lett.* **2005**, *5*, 2034. (c) Oubre, C.; Nordlander, P. *J. Phys. Chem. B* **2005**; *109*, 10042. (d) Wang, H.; Goodrich, G. P.; Tam, F.; Oubre, C.; Nordlander, P.; Halas, N. J. *J. Phys. Chem. B* **2005**, *109*, 11083.
(12) (a) Ambrose, W. P.; Goodwin, P. M.; Jett, J. H.; Van, Orden, A.; Werner, J. H.; Keller, R. A. *Chem. Rev.* **1999**, *99*, 2929. (b) Willets, K. A.; Nishimura, S. Y.; Schuck, P. J.; Twieg, R. J.; Moerner, W. E. *Acc. Chem. Res.* **2005**, *38*, 549. (c) Michalet, X.; Weiss, S.; Jager, M. *Chem. Rev.* **2006**, *106*, 1785.
(13) (a) Nie, S. *Single-Molecule Optical Detection, Imaging, and Spectroscopy*; Basche, T., Moerner, W. E., Orrit, M., Wild. U. P., Eds.; Wiley-VCH: New York. 1997. (c) Bokinsky, G.; Zhuang, X. *Acc. Chem. Res.* **2005**, *38*, 566.
(14) (a) Fu, Y.; Lakowicz, J. R. *Anal. Chem.* **2006**, *78*, 6238. (b) Fu, Y.; Lakowicz, J. R. *J. Phys. Chem. B* **2006**, *110*, 22557.
(15) (a) Hayat, M. A., Ed. *Colloidal Gold: Principles, Methods, and Applications*; Academic Press: San Diego, 1991. (b) Feldheim, D. L.; Foss, C. A. *Metal Nanoparticles: Synthesis, Characterization, and Applications*; Marcel Dekker: New York, 2002.
(16) Zhang, J.; Fu, Y.; Lakowicz, J. R. *J. Phys. Chem. C* **2007**, *111*, 50.
(17) (a) Kelly, K. L.; Coronado, E.; Zhao, L. L.; Schatz, G. C. *J. Phys. Chem. B* **2003**, *107*, 668. (b) Hao, E.; Li, S.; Bailey, R. C.; Zou, S.; Schatz, G. C.; Hupp, J. T. *J. Phys. Chem. B* **2004**, *108*, 1224.
(18) Taflove, A., Hagness, S. C. *Computational Electrodynamics: The Finite-Difference Time-Domain Method*; Artech House: Boston, 2000.
(19) Sullivan, D. M. *Electromagnetic Simulation Using the FDTD Method*; IEEE Press: New York, 2000.
(20) Yang, P.; Liou, N. K. *J. Opt. Soc. Am. A* **1996**, *13*, 2072.
(21) (a) Gray, S. K.; Kupka, T. *Phys. Rev. B* **2003**, *68*, 045415. (b) Chang, S.-H.; Gray, S. K.; Schatz, G. C. *Opt. Express* **2005**, *13*, 3150.
(22) Zhang, J.; Roll, D.; Geddes, C. D.; Lakowicz, J. R. *J. Phys. Chem. B* **2004**, *108*, 12210.
(23) (a) Huang, T.; Murray, R. W. *Langmuir* **2002**, *18*, 7077. (b) Huang, T.; Murray, R. W. *J. Phys. Chem. B* **2001**, *105*, 12498.
(24) Templeton, A. C.; Wuelfing, W. P.; Murray, R. W. *Acc. Chem. Res.* **2000**, *33*, 27.
(25) Ingram, R. S.; Hostetler, M. J.; Murray, R. W. *J. Am. Chem. Soc.* **1997**, *119*, 9175.
(26) Zhang, J.; Malicka, J.; Gryczynski, I.; Lakowicz, J. R. *J. Phys. Chem. B* **2005**, *109*, 7643.
(27) Rosi, N. L.; Mirkin, C. A. *Chem. Rev.* **2005**, *105*, 1547.
(28) Zhang, J.; Whitesell, J. K.; Fox, M. A. *Chem. Mater.* **2001**, *13*, 2323.

NL071084D